



## Measurement report: Secondary organic aerosols at a forested mountain site in southeastern China

Zijun Zhang<sup>1,2</sup>, Weiqi Xu<sup>1,\*</sup>, Yi Zhang<sup>1,2</sup>, Wei Zhou<sup>1</sup>, Xiangyu Xu<sup>1,2</sup>, Aodong Du<sup>1,2</sup>, Yinzhou Zhang<sup>1</sup>,  
Hongqin Qiao<sup>3</sup>, Ye Kuang<sup>3</sup>, Xiaole Pan<sup>1</sup>, Zifa Wang<sup>1,2</sup>, Xueling Cheng<sup>1</sup>, Lanzhong Liu<sup>4</sup>, Qingyan Fu<sup>5</sup>,  
5 Douglas R. Worsnop<sup>6</sup>, Jie Li<sup>1</sup>, Yele Sun<sup>1,2,\*</sup>

<sup>1</sup>State Key Laboratory of Atmospheric Boundary Layer Physics and Atmospheric Chemistry, Institute of Atmospheric Physics, Chinese Academy of Sciences, Beijing 100029, China

<sup>2</sup>College of Earth and Planetary Sciences, University of Chinese Academy of Sciences, Beijing 100049, China

<sup>3</sup>Institute for Environmental and Climate Research, Jinan University, Guangzhou 511143, China

10 <sup>4</sup>Shanghuang Atmospheric Boundary Layer and Eco-Environment Observatory, Institute of Atmospheric Physics, Chinese Academy of Sciences, Jinhua 321203, China

<sup>5</sup>Shanghai Environmental Monitoring Center, Shanghai 200235, China

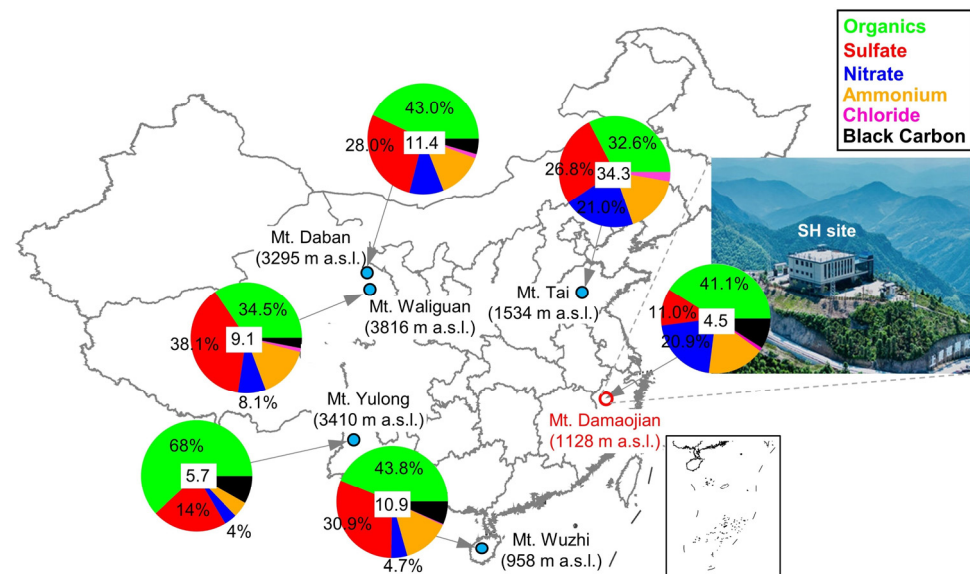
<sup>6</sup>Aerodyne Research Inc., Billerica, Massachusetts 01821, United States

Correspondence to: Weiqi Xu ([xuweiqi@mail.iap.ac.cn](mailto:xuweiqi@mail.iap.ac.cn)), Yele Sun ([sunyele@mail.iap.ac.cn](mailto:sunyele@mail.iap.ac.cn))

15 **Abstract.** Aerosol particles play crucial roles in both climate dynamics and human health. However, there remains a significant gap in our understanding of aerosol composition and evolution, particularly regarding secondary organic aerosols (SOA), and their interaction with clouds in high-altitude background areas in China. Here we conducted real-time measurements of submicron aerosols (PM<sub>1</sub>) using aerosol mass spectrometers at a forested mountain site (1128 m a.s.l.) in southeastern China in November 2022. Our results revealed that organic aerosol (OA) constituted a substantial portion of  
20 PM<sub>1</sub> (41.1 %), with the OA being primarily of secondary origin, as evidenced by a high oxygen-to-carbon (O/C) ratio (0.85–0.96). Positive matrix factorization resolved two distinct SOA factors: less oxidized oxygenated OA (LO-OOA) and more oxidized OOA (MO-OOA). Interestingly, MO-OOA was scavenged efficiently during cloud events, while cloud evaporation contributed significantly to LO-OOA. The ratio of OA/ $\Delta$ CO increased with a decrease in the O/C ratio, suggesting that OA  
25 remaining in cloud droplets generally maintained a moderate oxidation state. Furthermore, our results indicated a higher contribution of organic nitrates to total nitrate during cloudy periods (27 %) compared to evaporative periods (3 %). Notably, a substantial contribution of nitrate in PM<sub>1</sub> (20.9 %) was observed, particularly during high PM periods, implying that nitrate formed in polluted areas interacted with clouds and significantly impacted the regional background site. Overall, our study underscores the importance of understanding the dynamics of secondary organic aerosols and the impacts of cloud processing in regional mountainous areas in southeastern China.

### 30 1 Introduction

Aerosol particles play essential roles in regional and global climate (Ramanathan et al., 2001; Kanakidou et al., 2005), as well as air pollution (Huang et al., 2014) and public health (Kampa and Castanas, 2008). Submicron aerosol (PM<sub>1</sub>) from both



65

**Figure 1.** Location of the sampling site. The mean concentration (in  $\mu\text{g m}^{-3}$ ) and chemical composition of submicron aerosols (NR-PM<sub>1</sub>+BC if it was available) measured at selected mountain sites in China are also shown. Detailed information of these sampling sites is presented in Table S1 in the Supplement.

## 2 Methods

70

### 2.1 Site and instrumentation<sup>3</sup>

The campaign was carried out from 1 November to 30 November 2022 at Shanghuang Atmospheric Boundary Layer and Eco-Environment Observatory (SH site) on the top of Mt. Damaojian (119.51°E, 28.58°N, 1128 m a.s.l.) in Wuyi County, Zhejiang Province (Fig. 1). This site is a typical background site in southeastern China that is surrounded by mountains and forests, and there are no strong local anthropogenic sources nearby.

75

PM<sub>1</sub> species were measured using a suite of real-time instruments with 1–5 min time resolution, including an AMS operated under the “V-mode” and a quadrupole ACSM for non-refractory (NR)-PM<sub>1</sub> composition, together with a seven-wavelength Aethalometer (AE33, Magee Scientific Corp.) for equivalent black carbon (BC) mass concentration. The AMS measurements were only conducted during two periods (15–20 November and 24–28 November, respectively) in this study due to the malfunction of the instrument<sup>4</sup>. Briefly, aerosol particles were sampled into an air-conditioned room through

80

stainless steel tube (O.D.: 1/4 inch), and the residence time was estimated as 5 s. A nafion dryer was placed upstream of the ACSM and AMS to remove the moisture, after that, aerosol particles were sampled into AMS, ACSM, and AE33, respectively. Simultaneously, air pollutants including NO<sub>x</sub>, O<sub>3</sub>, PM<sub>2.5</sub>, and PM<sub>10</sub> were measured by gas analyzers<sup>5</sup> (Thermo Scientific Inc., USA), and CO was measured by a Picarro greenhouse gas analyzer (G2401, Picarro Inc., USA). In addition, meteorological parameters containing temperature (*T*), RH, wind speed (WS), wind direction (WD), and pressure (*P*) were

85

measured at the same site.<sup>6</sup>

## Page:3

Number: 1 Author: ADMIN Subject: Highlight Date: 2024-02-04 20:21:30

This is confusing, please make the caption more clearer by mentioning exactly at which site the measurements were carried out for this study.

Number: 2 Author: ADMIN Subject: Highlight Date: 2024-02-04 20:19:19

make it a superscript, check and rectify such discrepancies throughout the manuscript

Number: 3 Author: ADMIN Subject: Highlight Date: 2024-02-04 20:53:23

Please provide a table with all the instrumentation and corresponding periods

Number: 4 Author: ADMIN Subject: Highlight Date: 2024-02-04 20:23:05

What was the malfunction? and is the reported data checked and sanitised for possible errors?

Number: 5 Author: ADMIN Subject: Highlight Date: 2024-02-04 20:23:27

confusing, PM measured by what?

Number: 6 Author: ADMIN Subject: Highlight Date: 2024-02-04 20:23:54

by what?



## 2.2 Data analysis

### 2.2.1 ACSM and AMS

ACSM data were analyzed using ACSM standard data analysis software (v2.5.13) and AMS data were analyzed using  
90 SQUIRREL v1.65F and PIKA v1.25F. A composition-dependent collection efficiency (CDCE) was applied to the  
ACSM/AMS data according to Middlebrook et al. (2012). Elemental analysis of high-resolution mass spectra (HRMS) was  
performed using the “Improved-Ambient” (I-A) method (Canagaratna et al., 2015). The default relative ionization efficiency  
(RIE) values of 1.1, 1.4, and 1.3 were applied for nitrate, organics, and chloride. According to the ion efficiency (IE)  
calibration results, the RIE values of ammonium and sulfate were 5.05 and 0.73 for ACSM, and 5.26 and 1.28 for AMS,  
95 respectively. As shown in Fig. S1, the concentrations of NR-PM<sub>1</sub> tracked well with PM<sub>2.5</sub> and PM<sub>10</sub> measured by gas  
analyzers ( $r^2 = 0.70$  and  $0.66$ , respectively), suggesting that the AMS/ACSM quantification was reasonable.

PMF Evaluation Tool (PET v3.04) was employed to further deconvolve the HRMS into different source factors following  
the procedures reported by Ulbrich et al. (2009) and Zhang et al. (2011). In addition to organic fragment ions, the major  
fragment ions of inorganic species, i.e., SO<sup>+</sup> ( $m/z$  48), SO<sub>2</sub><sup>+</sup> ( $m/z$  64), SO<sub>3</sub><sup>+</sup> ( $m/z$  80), HSO<sub>3</sub><sup>+</sup> ( $m/z$  81), H<sub>2</sub>SO<sub>4</sub><sup>+</sup> ( $m/z$  98) for  
100 sulfate, NO<sup>+</sup> ( $m/z$  30), NO<sub>2</sub><sup>+</sup> ( $m/z$  46) for nitrate, NH<sup>+</sup> ( $m/z$  15), NH<sub>2</sub><sup>+</sup> ( $m/z$  16), NH<sub>3</sub><sup>+</sup> ( $m/z$  17) for ammonium, and Cl<sup>+</sup> ( $m/z$   
35), HCl<sup>+</sup> ( $m/z$  36) for chloride were also included into the HR data and error matrices for PMF. A more detailed description  
of the procedures was given in Sun et al. (2012). After checking the key diagnostic plots (Fig. S2), mass spectra, and the  
correlations with related tracers, a four-factor solution was considered as the optimal solution in this study.

### 2.2.2 Estimation of organic nitrates

105 ONs were estimated from the PMF results (Zhang et al., 2011; Xu et al., 2015). Briefly, NO<sub>x</sub><sup>+</sup> (i.e., NO<sup>+</sup> and NO<sub>2</sub><sup>+</sup>) are major  
fragments of nitrate functionality (-ONO<sub>2</sub>), which can be referred to as the total nitrate measured by AMS. Combining  
inorganic with organic mass spectra in PMF, NO<sup>+</sup> and NO<sub>2</sub><sup>+</sup> can be separated into different organic aerosol (OA) factors and  
an inorganic nitrate aerosol factor (NIA). Therefore, the mass concentration of ONs (NO<sub>3,org</sub>) was calculated by summing  
these two ion signals distributed in all OA factors as follows:

$$110 \text{ NO}_{3,\text{org}} = \text{NO}_{\text{org}}^+ + \text{NO}_{2,\text{org}}^+ \quad (1)$$

$$\text{NO}_{\text{org}}^+ = \sum([\text{OA factor}]_i \times f_{\text{NO}^+,i}) \quad (2)$$

$$\text{NO}_{2,\text{org}}^+ = \sum([\text{OA factor}]_i \times f_{\text{NO}_2^+,i}) \quad (3)$$

where [OA factor]<sub>*i*</sub> represents the mass concentration of OA factor *i* resolved by PMF,  $f_{\text{NO}^+,i}$  and  $f_{\text{NO}_2^+,i}$  are the mass fractions  
of NO<sup>+</sup> and NO<sub>2</sub><sup>+</sup> in OA factor *i*, respectively.

## Page:4

 Number: 1 Author: ADMIN Subject: Highlight Date: 2024-02-04 20:24:59  
PM measured by gas analyzers? provide clear description in the methodology part.

 Number: 2 Author: ADMIN Subject: Highlight Date: 2024-02-04 20:25:30  
and slopes?

 Number: 3 Author: ADMIN Subject: Highlight Date: 2024-02-04 20:27:34  
ON could also be estimated using NO+/NO2+ ratios as reported in some studies, so why PMF?



### 115 2.2.3. Backward trajectory analysis

The Hybrid Single-Particle Lagrangian Integrated Trajectories (HYSPLIT) model and meteorological data from the NOAA Global Data Assimilation System (GDAS) were used to calculate 72 h backward trajectories at the SH site. The trajectory time was set from 0:00 to 23:00 at 1 h intervals, and the height was set as 1100 m. To further show the particle concentration levels in different regions, the map was colored by the time-averaged organic carbon surface mass concentration (ENSEMBLE) from the MERRA-2 model, which was obtained from the NASA Giovanni website (<http://giovanni.sci.gsfc.nasa.gov/giovanni>).

## 3. Results and discussion

### 3.1. General descriptions

Figure 2 shows the time series of meteorological parameters ( $T$ , RH, WD, and WS), air pollutants ( $PM_{2.5}$  and CO) along with  $PM_{10}$  species during the campaign. The total  $PM_{10}$  concentration varied dynamically from  $0.3 \mu\text{g m}^{-3}$  to  $57.95 \mu\text{g m}^{-3}$  with an average ( $\pm 1\sigma$ ) of  $4.45 \pm 6.51 \mu\text{g m}^{-3}$ . As shown in Fig. 1, organics held the largest contribution to total  $PM_{10}$  during the sampling period (41.1 %), followed by nitrate (20.9 %), ammonium (17.0 %), sulfate (11.0 %), BC (9.0 %), and chloride (1.0 %). The concentration and composition of  $PM_{10}$  are quite different from those observed at other mountain sites with similar altitudes (Fig. 1), such as Mt. Wuzhi, where  $PM_{10}$  has a mean mass concentration of  $10.9 \mu\text{g m}^{-3}$ , and sulfate makes up a significant part (30.9 %) of total  $PM_{10}$  (Zhu et al., 2016). Note that the  $PM_{10}$  concentration at SH site is even lower than those at mountain sites with higher altitude (Fig. 1), such as Mt. Tai ( $34.3 \mu\text{g m}^{-3}$ ) in NCP (Zhang et al., 2014), Mt. Yulong ( $5.4 \mu\text{g m}^{-3}$ ) (Zheng et al., 2017), and Mt. Waliguan ( $9.1 \mu\text{g m}^{-3}$ ) (Zhang et al., 2019). Considering the occurrence of frequent cloud events during the sampling period, the low  $PM_{10}$  concentration might be mainly associated with cloud scavenging (Kim et al., 2019). Indeed, the unexpectedly high fraction of nitrate at the regional background site might indicate that nitrate formed from anthropogenic-emitted  $NO_x$  can have a significant impact on regional scale in the southeastern China. One explanation was that nitrate formed in polluted regions interacted with clouds and affected the regional nitrate level as cloud evaporates (Tao et al., 2018).

Figure 3 shows the relative contribution of each  $PM_{10}$  component as a function of  $PM_{10}$  concentration together with the probability density of  $PM_{10}$  mass loading. The highest two probabilities were distributed within  $0\text{--}6 \mu\text{g m}^{-3}$  and  $12\text{--}18 \mu\text{g m}^{-3}$  (48.5 % and 30.1 %, respectively). The fraction of nitrate increased significantly with  $PM_{10}$  concentration, and meanwhile, the fraction of organics and BC exhibited a decreasing trend. This result suggested that high levels of  $PM_{10}$  at the SH site might be mainly attributed to the nitrate formation and transport. It is also noted that a nitrate-dominant peak of  $PM_{10}$  mass loading was observed at the nighttime of 4 November (Fig. 2d), which was associated with the corresponding increase in CO, further emphasizing the contribution of transport to nitrate.



155 The diurnal cycles of PM<sub>1</sub> species, air pollutants, and meteorological parameters during the entire campaign are illustrated in Fig. S3. The mean and median values of organics and nitrate both showed distinct noon peaks at around 14:00, which could be attributed to the daytime photochemical production and the low wind speed (Tang et al., 2022; Xu et al., 2018b). The high nighttime peak of nitrate was mainly due to the influences of the nitrate event on 4 November. Comparatively, sulfate, chloride, and BC showed relatively flat diurnal variations, suggesting the regional characteristics of these species (Zhang et al., 2015).

### 3.2 Comparisons of two different periods

160 RH plays a crucial role in determining the composition, formation, and evolution of PM<sub>1</sub> (Sun et al., 2013; Xu et al., 2019). Figure S4 shows the variation of organics, nitrate, and sulfate mass concentrations as a function of RH during the entire campaign. Overall, the mass concentrations of organics decreased significantly with increasing RH, while nitrate and sulfate only showed slight decreases. Previous studies have shown that aerosol mass generally increases on foggy days (Chen et al., 2021). This phenomenon could be due to the cloud scavenging effect under high RH at this site. Another explanation is that  
165 submicron aerosols grow to larger sizes under high RH that AMS aerodynamic lens cannot transmit (Chakraborty et al., 2016). To further investigate aerosol characteristics under different meteorological conditions, we selected two periods (Fig. 2, denoted as P1 and P2 hereafter) with largely different humidity and PM<sub>1</sub> concentrations. P1 was a typical cloud scavenging period with relative humidity remaining to be saturated (RH = 100 %), and meanwhile, PM<sub>1</sub> stayed at a very low level, with an average value of 1.34 μg m<sup>-3</sup>. Whereas in P2, the mean RH decreased to 93.9 % with almost no cloud event,  
170 and a high PM<sub>1</sub> event happened with a maximum mass concentration of 20.65 μg m<sup>-3</sup> (an average 9.39 μg m<sup>-3</sup>). Then, the PM<sub>1</sub> concentration decreased rapidly due to the enhanced mountain-valley wind (WS > 4 m s<sup>-1</sup>) and increasing RH (71 % to 100 %) during the nighttime. Therefore, P2 was more likely to be a cloud evaporation period, where aerosol particles were released from the cloud droplets after water evaporation (Fanourgakis et al., 2019).

#### 3.2.1 Size distributions and composition

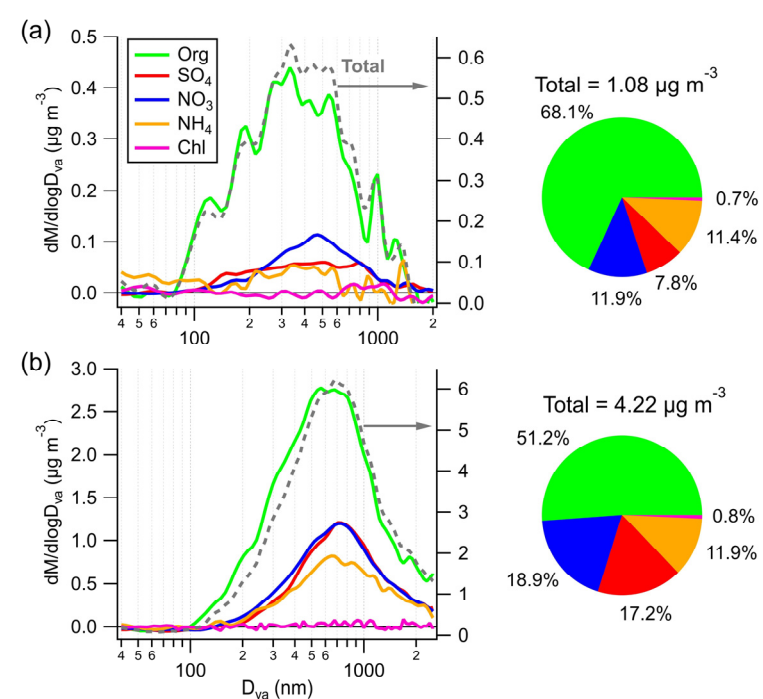
175 The average chemically resolved size distributions of NR-PM<sub>1</sub> during P1 and P2 are shown in Fig. 4. Generally, all species were distributed in accumulation mode in both periods. However, a smaller peak size (300–500 nm) and broader size distribution were observed during P1 when compared to those of P2 (~700 nm), probably owing to the wet removal of larger and hygroscopic particles in P1 (Ge et al., 2012). Ammonium showed similar size distribution with sulfate and nitrate during P2, while in P1, it was mixed mainly with sulfate and exhibited a quite different size distribution with nitrate, indicating the  
180 potential contribution of organic nitrate.

Clear differences were also found in aerosol composition during P1 and P2. Organics were the dominant contributor to total NR-PM<sub>1</sub> mass during P1 (68 %), followed by nitrate (12 %), ammonium (11 %), and sulfate (8 %). In contrast, despite the decreased contribution of organics (51 %), the mass fractions of sulfate and nitrate increased considerably during P2 (17 % and 19 %, respectively). These changes in the mass fraction of species were attributed to the lower mass scavenging

Number: 1 Author: ADMIN Subject: Highlight Date: 2024-02-04 20:34:44  
High PM1 even had 20.65 ug/m3 max conc. then when that 57.95 ug/m3 IPM1 level event happened?

Number: 2 Author: ADMIN Subject: Highlight Date: 2024-02-04 20:38:55  
I am not convinced with the identification/naming of P1 and P2 events, evidences are not clear to term them as cloud and evaporating cloud episodes. Rh 100% or 90% doesn't necessarily indicating cloud or its evaporation.

185 efficiency of organics than inorganic species (Gilardoni et al., 2014). The average HRMS of OA during P1 and P2 are  
 presented in Fig. S5. The HRMS of OA were quite similar for the two periods, with a significant peak  $m/z$  44 (mainly  $\text{CO}_2^+$ ).  
 The OA was highly oxidized, with  $\text{C}_x\text{H}_y\text{O}_1^+$  dominating the total OA in P1 and P2 by 41 % and 40 %, followed by  $\text{C}_x\text{H}_y^+$   
 (31 % and 32 %), and  $\text{C}_x\text{H}_y\text{O}_2^+$  (20 % and 19 %). The contributions of the two major oxygen-containing ion fragments  
 ( $\text{C}_x\text{H}_y\text{O}_1^+$  and  $\text{C}_x\text{H}_y\text{O}_2^+$ ) at the SH site were much higher than those at various urban or suburban sites in China, such as 37.4 %  
 190 in urban Nanjing (Wang et al., 2016), and 52.9 % in suburban Lanzhou (Tang et al., 2022). Note that higher fraction of  $\text{CO}_2^+$   
 (3 % higher) was found in P1 than P2 (Fig. S5c), indicating a higher oxidation degree of OA in P1 (Xu et al., 2014). This is  
 consistent with the higher O/C and OSc (0.96 and 0.49) in P1 than P2 (0.85 and 0.21).<sup>1</sup>



195 **Figure 4.** Averaged size distributions and chemical composition of NR-PM<sub>1</sub> during (a) P1 and (b) P2.

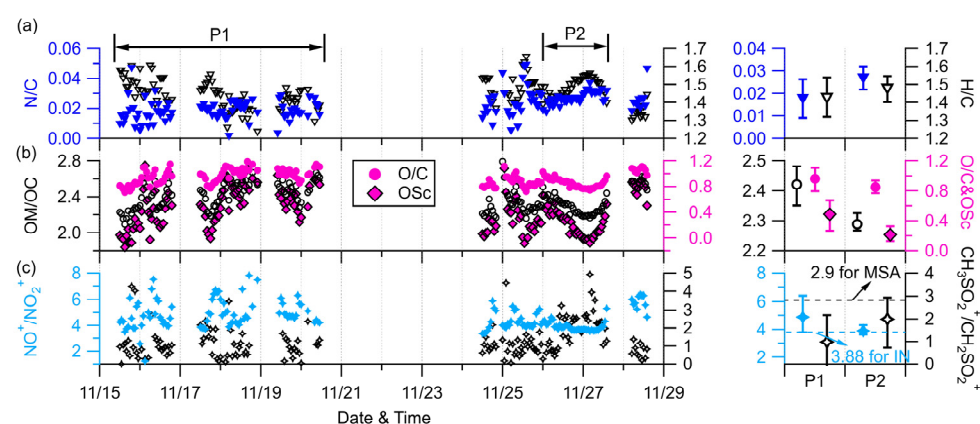
### 3.2.2 Elemental ratios

Figure 5 shows the time series and box plots of N/C, H/C, OM/OC, O/C, and carbon oxidation state (OSc) of OA, as well as  
 two ion ratios at the SH site. The hourly averaged ratios were only reported for periods with OA concentrations above 0.7  $\mu\text{g}$   
 200  $\text{m}^{-3}$ . The average N/C ratios were 0.018 for P1 and 0.027 for P2, consistent with the higher fraction of  $\text{C}_x\text{H}_y\text{N}_p^+$  in OA during  
 P2. OA had a slightly lower H/C ratio (1.44 vs. 1.48) and higher average ratios of O/C (0.96 vs. 0.85), OM/OC (2.42 vs.  
 2.29), and OSc (0.49 vs. 0.21) during P1 than those during P2, indicating more oxidized OA during P1. The O/C ratios were



overall within the range of  $0.94 \pm 0.18$  at regional background sites (Zhou et al., 2020), yet much higher than those observed at urban and suburban sites. These results suggest that OA at the SH site was relatively ~~well~~ aged.

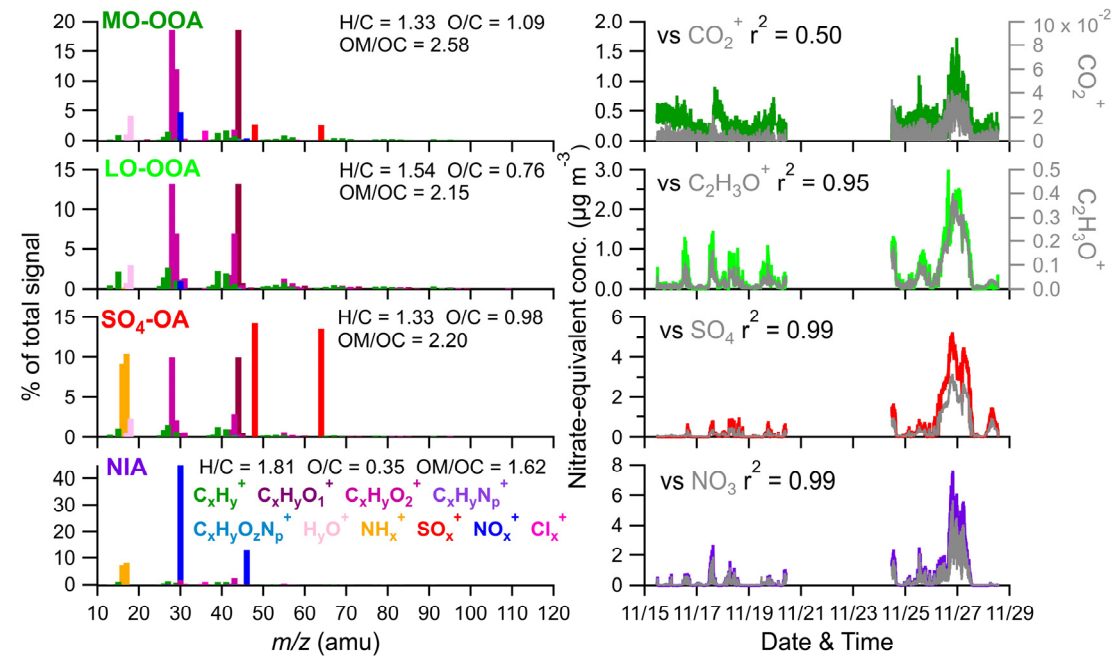
205 The ratio of fragment ions  $\text{NO}^+$  ( $m/z$  30) to  $\text{NO}_2^+$  ( $m/z$  46) is a good indicator for identifying the presence of ONs (Farmer et al., 2010; Lin et al., 2021). The mean ratio of  $\text{NO}^+/\text{NO}_2^+$  in P1 was 4.9, which exceeds the value of 3.88 for pure  $\text{NH}_4\text{NO}_3$  (AN) obtained from the AMS IE calibration, indicating a potential contribution of ONs. Conversely, the mean  $\text{NO}^+/\text{NO}_2^+$  in P2 (3.9) was almost identical to that of AN, implying the dominance of inorganic nitrates (INs). Additionally, the  $\text{CH}_2\text{SO}_2^+$  ( $m/z$  79) and  $\text{CH}_3\text{SO}_2^+$  ( $m/z$  80) ions were used as signature fragments of methanesulfonate, a typical organic sulfur species  
 210 (Chen et al., 2019). However, the mean ratios of  $\text{CH}_3\text{SO}_2^+$  and  $\text{CH}_2\text{SO}_2^+$  during P1 and P2 (0.98 and 1.99, respectively) were lower than the value of 2.9 reported in previous studies for MSA, **indicating the negligible contribution of MSA** (Song et al., 2019).



215 **Figure 5.** Time series and box plots of 1-hour averaged (a) N/C and H/C, (b) OM/OC, OSc, and O/C, and (c)  $\text{NO}^+/\text{NO}_2^+$  and  $\text{CH}_3\text{SO}_2^+/\text{CH}_2\text{SO}_2^+$ . Only ratios determined with good S/N (i.e., organics  $> 0.7 \mu\text{g m}^{-3}$ ) are shown.

### 3.3 Source apportionment of OA and contribution of organic nitrates

Four factors were resolved by PMF, including three types of SOA and one inorganic factor: less oxidized oxygenated OA (LO-OOA), more oxidized oxygenated OA (MO-OOA), OA associated with sulfate ions ( $\text{SO}_4\text{-OA}$ ), and inorganic nitrate aerosol (NIA). These four factors together on average accounted for 87.5 % of the total NR- $\text{PM}_{10}$  mass. The mass spectra profiles and OA ion family composition of the four factors are shown in Figs. 6 and 7.



225 **Figure 6.** High-resolution mass spectral profiles (left) and time series (right) of four factors. The correlations of four factors with corresponding tracers are also shown. <sup>1</sup>

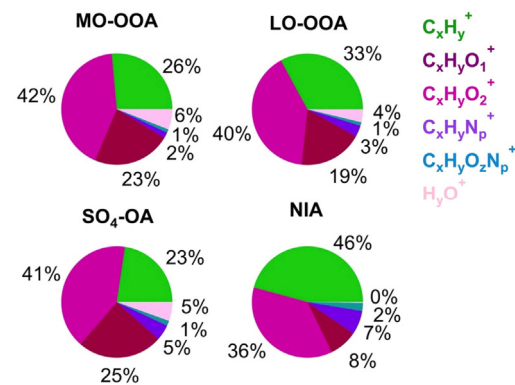


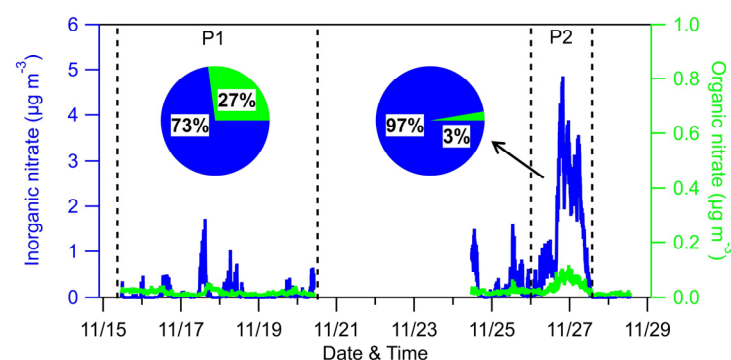
**Figure 7.** Mass fractional composition of OA ion families for the resolved four PMF factors.

230 LO-OOA and MO-OOA were identified by prominent peaks of  $\text{CO}^+$  and  $\text{CO}_2^+$  in the mass spectra. LO-OOA had a high  
 fraction of  $\text{C}_2\text{H}_3\text{O}^+$  ( $m/z$  43, 6.8 % of the total signal), while MO-OOA, corresponding to more oxidized and aged  
 components, had a higher abundance of  $\text{CO}_2^+$  (17.6 % vs. 12.8 %),  $\text{C}_x\text{H}_y\text{O}_2^+$  (23 % vs. 19 %), and O/C ratio (1.09 vs. 0.76)  
 than LO-OOA. The average O/C ratios of these two OOA factors are similar to those at Mt. Bachelor, where the O/C ratios  
 of SV-OOA and LV-OOA were 0.67 and 1.17, respectively (Zhou et al., 2019). LO-OOA correlated tightly with  $\text{C}_2\text{H}_3\text{O}^+$  ( $r^2$   
 235 = 0.95), and MO-OOA showed a moderate correlation with sulfate ( $r^2 = 0.56$ ). Overall, the LO-OOA and MO-OOA





components account for 39.1 % and 29.4 % of the total measured OA mass, respectively (Fig. S6). The mass spectra of the  $\text{SO}_4\text{-OA}$  factor had a large amount of  $\text{NH}_x^+$  and  $\text{SO}_x^+$ , together accounting for 48.5 % of the total mass of this factor. Meanwhile, organic components also made up a considerable fraction, yet on average contributing 51 %. It is also noticed that the O/C ratio of the organic fraction of this factor is 0.98, which is even higher than LO-OOA and comparable to MO-OOA, suggesting that this factor has experienced aging processes during the regional transport. Not surprise, no primary OA factor (e.g., hydrocarbon-like OA, biomass burning OA, etc.) was resolved during this study due to the negligible influences of local emissions, which was consistent with the PMF results at other background sites (Zhou et al., 2019; Zhu et al., 2016). A nitrate aerosol factor was also separated from these OA factors, with nitrates in this factor accounting for 92.6 % of the total  $\text{NO}_x^+$  ions. Despite NIA,  $\text{NO}_x^+$  ions were more assigned in MO-OOA (6.0 % of the total  $\text{NO}_x^+$ ) than LO-OOA (1.4 % of the total  $\text{NO}_x^+$ ), suggesting that ONs were more associated with MO-OOA. According to previous studies, the ratios of  $\text{NO}^+/\text{NO}_2^+$  for ONs are approximately 2.25–3.7 times higher than pure  $\text{NH}_4\text{NO}_3$  (Fry et al., 2013; Fry et al., 2009). Consistently, the average  $\text{NO}^+/\text{NO}_2^+$  ratios of LO-OOA and MO-OOA were 13.19 and 11.2, falling within the range of ONs. In contrast, a  $\text{NO}^+/\text{NO}_2^+$  ratio of 3.56 was observed for NIA, reflecting its characteristics of inorganic nitrates. Based on the PMF results above, the mass concentrations of ONs during the AMS sampling period were estimated (Fig. 10). Considering ONs as part of organics, we chose a RIE value of 1.4 for the estimated ONs, while a nitrate RIE value (1.1) was correspondingly applied for INs. The results showed that ONs made a greater contribution to total nitrate in P1 than in P2 (27 % vs. 3 %). This was further supported by the result of Huang et al. (2021), which found that organic nitrate can increase rapidly when  $\text{RH} > 70\%$ . The average mass concentration of ONs in P1 was  $30 \text{ ng m}^{-3}$ , which was comparable to that in P2 ( $40 \text{ ng m}^{-3}$ ), likely owing to the cloud scavenging. Also, the ONs at this site was close to the value ( $40 \text{ ng m}^{-3}$ ) obtained at a forest-urban mixed site in Finland (Hao et al., 2014). However, significant discrepancies were observed between the INs mass concentrations during P1 and P2 ( $0.08 \text{ } \mu\text{g m}^{-3}$  vs.  $1.47 \text{ } \mu\text{g m}^{-3}$ ), revealing that INs dominated the elevation of total nitrate during cloud evaporation in P2.



260 **Figure 8.** Time series and relative contributions of inorganic nitrate and organic nitrate during the AMS sampling period.



### 3.4 Evolution of OA

The formation and evolution of OA can be investigated using the ratio of OA to  $\Delta\text{CO}$  (CO minus background CO) to remove the atmospheric dilution effects (Sun et al., 2011). In this study, 0.12 ppmv (average of the lowest 5 % concentration) was used as the background mixing ratio of CO (Fig. S7), which is close to the 0.1 ppm used in Hu et al. (2013) and Yuan et al. (2013). OA/ $\Delta\text{CO}$  was  $28.3 \pm 26.3 \mu\text{g m}^{-3} \text{ppmv}^{-1}$  during the studying period, which is comparable to  $(41.7 \pm 23.0 \mu\text{g m}^{-3} \text{ppmv}^{-1})$  in suburban Sichuan Basin (Hu et al., 2016) but much lower than the mean value  $(70 \pm 20 \mu\text{g m}^{-3} \text{ppmv}^{-1})$  in worldwide urban air (De Gouw and Jimenez, 2009). The scatter plot of OA/ $\Delta\text{CO}$  as a function of O/C ratios during P1 and P2 is shown in Fig. 9a. Interestingly, different OA/ $\Delta\text{CO}$  variations were found with the increasing O/C during P1 and P2. During P1, OA/ $\Delta\text{CO}$  trended to increase with the increase of the O/C ratio, indicating aging process produced SOA (Hu et al., 2017). In contrast, a remarkable decrease trend of OA/ $\Delta\text{CO}$  was observed with the increasing O/C during P2, suggesting that less oxidized OA may contribute more significantly to the high OA concentration during this period. Moreover, the negative correlation between OA/ $\Delta\text{CO}$  and O/C in P2 also implies that more oxidized OA had almost been scavenged by clouds, while less oxidized OA previously formed or scavenged into cloud droplets was released during cloud evaporation. Similarly, significant increases in the LO-OOA concentration (0.27 to  $1.70 \mu\text{g m}^{-3}$ ) and fraction (40 % to 70 %) were observed from P1 to P2, while the MO-OOA concentration (0.40 vs.  $0.74 \mu\text{g m}^{-3}$ ) did not show large variation (Fig. 9b), further supporting our conclusion. In addition, these released LO-OOA is likely composed of humic-like substances (HULIS), which can account for 49 % of the water-soluble organic matter at a nearby mountain site in southeastern China (Tao et al., 2023; Chen et al., 2016).

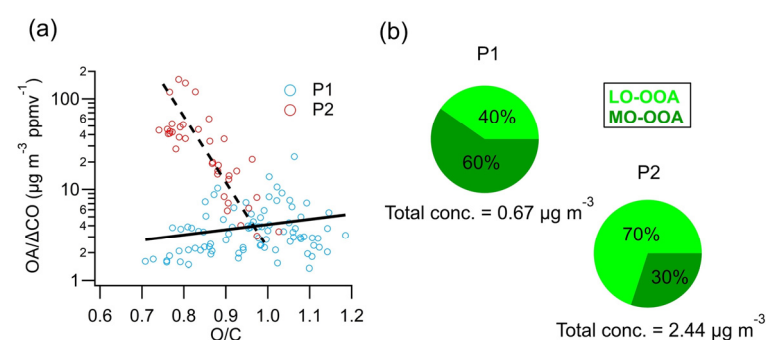


**Figure 9.** (a) Scatter plot of OA/ $\Delta\text{CO}$  as a function of O/C ratios and (b) mass concentrations and proportions of MO-OOA and LO-OOA during P1 and P2.

Figure 10a shows the Van Krevelen diagrams of OA in this study together with other mountain sites. The slope of H/C to O/C in the present study was -0.66 ( $r^2 = 0.64$ ), suggesting the addition of carboxyl functional groups during OA evolution (Heald et al., 2010). It is interesting to mention that the two OOA factors exhibited a strong alignment with the fitting line, which suggested that the evolution of OA in this site likely follows a transformation pathway from LO-OOA to MO-OOA.